Neuron, Vol. 44, 663–676, November 18, 2004, Copyright ©2004 by Cell Press

The Translational Repressor Pumilio Regulates Presynaptic Morphology and Controls Postsynaptic Accumulation of Translation Factor eIF-4E

Kaushiki P. Menon,[1] Subhabrata Sanyal,[2] Yasuaki Habara,[3] Ricardo Sanchez,[3] Robin P. Wharton,[3] Mani Ramaswami,[2] and Kai Zinn[1,*]
[1]Division of Biology
California Institute of Technology
Pasadena, California 91125
[2]Department of Molecular and Cellular Biology and ARL Division of Neurobiology
University of Arizona
Tucson, Arizona 85716
[3]Howard Hughes Medical Institute
Department of Molecular Genetics and Microbiology
Duke University Medical Center
Durham, North Carolina 27710

Summary

Translational repression by *Drosophila* Pumilio (Pum) protein controls posterior patterning during embryonic development. Here, we show that Pum is an important mediator of synaptic growth and plasticity at the neuromuscular junction (NMJ). Pum is localized to the postsynaptic side of the NMJ in third instar larvae and is also expressed in larval neurons. Neuronal Pum regulates synaptic growth. In its absence, NMJ boutons are larger and fewer in number, while Pum overexpression increases bouton number and decreases bouton size. Postsynaptic Pum negatively regulates expression of the translation factor eIF-4E at the NMJ, and Pum binds selectively to the 3′UTR of *eIF-4E* mRNA. The GluRIIa glutamate receptor is upregulated in *pum* mutants. These results, together with genetic epistasis studies, suggest that postsynaptic Pum modulates synaptic function via direct control of eIF-4E expression.

Introduction

The *Drosophila* larval neuromuscular junction (NMJ) uses glutamate as its major neurotransmitter and employs ionotropic glutamate receptors (GluRs) homologous to vertebrate AMPA receptors. The NMJ is organized into distinct motor axon varicosities known as boutons, and its synapses exhibit plastic behavior during development. The NMJ's postsynaptic scaffold contains a functional ortholog of the mammalian PSD-95 protein, as well as relatives of other mammalian postsynaptic density components (Keshishian et al., 1996; Koh et al., 2000). These properties make the fly NMJ a useful genetic model system for the study of excitatory synapses in the mammalian brain.

Larval NMJs grow extensively in order to adjust to the large increases in the surface area of their muscle targets that occur between the first and third instar stages (Lnenicka and Keshishian, 2000). The number of boutons at an NMJ increases by up to 10-fold, and new active zones are added to each bouton. Boutons are added by a process of budding. New boutons emerge at the ends of NMJ branches or intercalate between two existing boutons within a branch (Zito et al., 1999).

The NMJ can also rapidly increase in strength in response to larval motor activity, and this strengthening is accompanied by local increases in postsynaptic proteins. A few hours after formerly sluggish larvae begin to move vigorously, aggregates of the translation factors eIF-4E and polyA binding protein (PABP) appear at their NMJs. Spots of intense GluR labeling (puncta) appear at new sites, and additional presynaptic active zones are recruited to these puncta. Finally, new boutons are added to the NMJ (Sigrist et al., 2000, 2003).

The appearance of new spots of translation factors and GluR after induction of movement is consistent with the hypothesis (see Discussion) that local translation contributes to synaptic plasticity at the *Drosophila* NMJ. Local translation at synapses has been studied in *Aplysia*, mammalian, and arthropod systems. It has attracted interest as a mechanism that allows neurons to separately adjust the strengths of individual synapses (Steward and Schuman, 2001).

Polysomes and other components of the translational machinery are located at the bases of dendritic spines in mammalian brain neurons, and a specific subset of mRNAs is localized to dendrites. These mRNAs encode proteins that are important for synaptic function, including the NR1 subunit of the NMDA receptor and the α subunit of CaM kinase II. Synaptic input can activate local translation of dendritic mRNAs by a number of different mechanisms. One of these involves eIF-4E, which is held in an inactive state by binding proteins called 4E-BPs. 4E-BPs are phosphorylated in response to activation of the Target-of-Rapamycin (TOR) kinase, and this causes them to dissociate from eIF-4E. TOR activity is required for local translation in mammalian and *Aplysia* systems (Jiang and Schuman, 2002).

We became interested in translational control of synaptic growth and function through a screen for genes that affect larval NMJ morphology when overexpressed in neurons. In this screen, we identified ten genes encoding RNA binding proteins. This finding suggested that these genes might regulate translation, transport, localization, or stability of mRNAs involved in synaptic development. Among them are the known genes *pumilio* (*pum*), *egalitarian*, and *apontic*, whose products are involved in mRNA localization and translation in oocytes and early embryos (Kraut et al., 2001).

Pum is well known for its role in determination of abdominal segmentation in the early embryo. Maternally synthesized *hunchback* (*hb*) mRNA is distributed throughout the embryo, but Hb protein must be excluded from the posterior region to permit normal abdominal development. Maternal Pum binds to sequences (NREs) in the 3′UTR of *hb* mRNA (Murata and Wharton, 1995), and the resulting Pum-RNA complex subsequently recruits two additional cofactors, Nanos

*Correspondence: zinnk@caltech.edu

and Brain Tumor, into a quaternary complex (Sonoda and Wharton, 1999, 2001). This assembly then blocks translation by as yet unknown mechanisms (Chagnovich and Lehmann, 2001). The RNA binding PUF domain of Pum is shared by proteins in many species, and all other characterized PUF proteins are also posttranscriptional regulators of gene expression (Wickens et al., 2002).

Pum has closely related human orthologs that are expressed in the brain (Spassov and Jurecic, 2003). The functions of vertebrate Pums are unknown, but they can form complexes with a variety of other proteins. Interestingly, one of these is CPEB (cytoplasmic polyadenylation element binding protein), which controls translation of synaptic mRNAs (Nakahata et al., 2001). CPEB binding sites in the 3′UTR of *CaMKIIα* mRNA are required for transmitter-induced CaMKIIα expression in dendrites (Jiang and Schuman, 2002; Wells et al., 2001).

Drosophila Pum is required zygotically as well as maternally, but its roles in later development are not well understood. However, several studies have implicated Pum in neuronal development and function. In our screen, we found that neuronal overexpression of a C-terminal Pum fragment from an EP element (Rorth et al., 1998) alters larval NMJs (Kraut et al., 2001). A hypomorphic P element insertion mutation produces a hyperexcitability phenotype in larval motor neurons (Schweers et al., 2002). Similar hypomorphic *pum* alleles were found to affect associative memory formation in adult flies (Dubnau et al., 2003). Finally, a recent paper demonstrates that Pum is involved in dendritic morphogenesis in larval peripheral sensory neurons (Ye et al., 2004).

In this paper, we examine Pum's functions in neuromuscular system development by analyzing *pum* loss-of-function (LOF) phenotypes and characterizing its expression patterns. We show that Pum has distinct pre- and postsynaptic roles at the larval NMJ. In neurons, Pum regulates synaptic growth and morphology. In muscles, postsynaptic Pum controls local accumulation of eIF-4E.

Results

Pumilio Is Cytoplasmic in Neurons and Localized to the NMJ in Muscles

To analyze Pum's expression patterns in third instar larvae, we used two polyclonal antibodies, made in different species by different groups, that recognize nonoverlapping regions of the protein. One of these (anti-PumN; rabbit) was raised against amino acids (aa) 408–883 of the unique N-terminal region of the protein (Forbes and Lehmann, 1998), while the other (anti-PumRBD; rat) is against the PUF RNA binding domain (RBD; aa 1093–1533) (Sonoda and Wharton, 1999).

For staining experiments and studies of mutant phenotypes (see below), we used transheterozygotes involving three *pum* alleles (pum^{ET9}, pum^{ET7}, and pum^{Msc}) together with a deficiency mutation, *Df(3R)BSC24*. pum^{ET9} and pum^{ET7} are ethyl methane sulfonate (EMS)-induced nonsense mutations within the RBD coding region, while pum^{Msc} is an inversion with one breakpoint in the large eighth intron of the *pum* gene. All three alleles produce strong maternal phenotypes (Forbes and Lehmann, 1998), but it is unknown whether any *pum* allele is a genetic null. In our experiments, pum^{Msc}, in which the RBD coding region is intact, conferred weaker morphological and electrophysiological phenotypes than the other mutant chromosomes. We found that there are no *pum* alleles that are protein null in larvae; all *pum* genotypes retain residual protein expression in both neurons and muscle (see below).

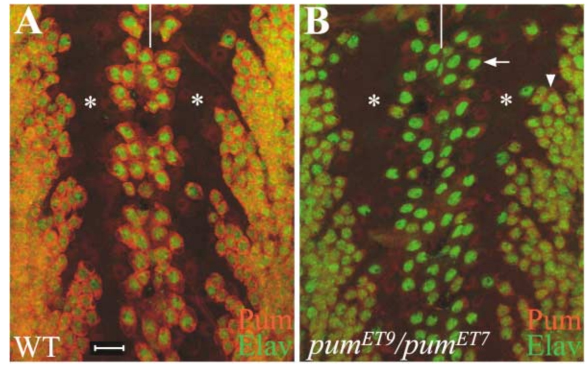

Figure 1. Pumilio Is Localized to the Cytoplasm of Neurons in the Larval Ventral Nerve Cord

The larval ventral nerve cord (VNC) in wild-type (A) and in a pum^{ET9}/pum^{ET7} mutant (B) was stained with anti-PumN (red) and anti-Elav (green), and staining was visualized with confocal microscopy. (A) Pum staining surrounds staining for the neuronal nuclear marker Elav in most or all CNS neurons. Asterisks indicate the regions occupied by axon tracts. Vertical lines at the top of the panels indicate the position of the midline. (B) In pum^{ET9}/pum^{ET7} larvae, Pum staining is almost undetectable in medially located neurons (arrow) and is reduced in laterally located neurons (arrowhead). Scale bar, 10 μm.

We stained dissected larval "fillet" preparations with anti-PumN and anti-Pum-RBD, using fluorescent secondary antibodies and confocal microscopy for visualization, and compared staining between wild-type and two strong mutant genotypes, pum^{ET9}/pum^{ET7} and pum^{ET7}/*Df(3R)BSC24*. Figure 1 shows larval ventral nerve cords (VNCs) of w^{1118}, used as a "wild-type" control, and pum^{ET9}/pum^{ET7}, double stained with anti-PumN and an antibody against the neuronal nuclear protein Elav. Pum is expressed in the cytoplasm of most or all CNS neurons, and the staining pattern has a vesicular appearance. In medially located neurons, Pum is undetectable in *pum* mutant larvae (arrow), while low levels are still present in more lateral neurons (arrowhead). Similar results were obtained with the other antibody, anti-PumRBD, and with pum^{ET7}/*Df(3R)BSC24* larvae (data not shown).

In muscles, Pum is localized to domains surrounding NMJ boutons. Figure 2A shows confocal z series projections of wild-type (w^{1118}) muscle 4 NMJs double stained with anti-PumN and anti-Discs-large (Dlg), a primarily postsynaptic marker protein localized to the subsynaptic reticulum (SSR) that underlies each bouton. Pum is expressed at both type Ib and type Is boutons (Figure 2A1). Both of these bouton types contain glutamatergic synapses. Ib boutons (arrow in Figure 2A1) can be recognized by their larger size and higher level of Dlg expression relative to Is boutons (arrowhead in Figure 2A1). Pum and Dlg appear to colocalize at both bouton types (Figure 2A3).

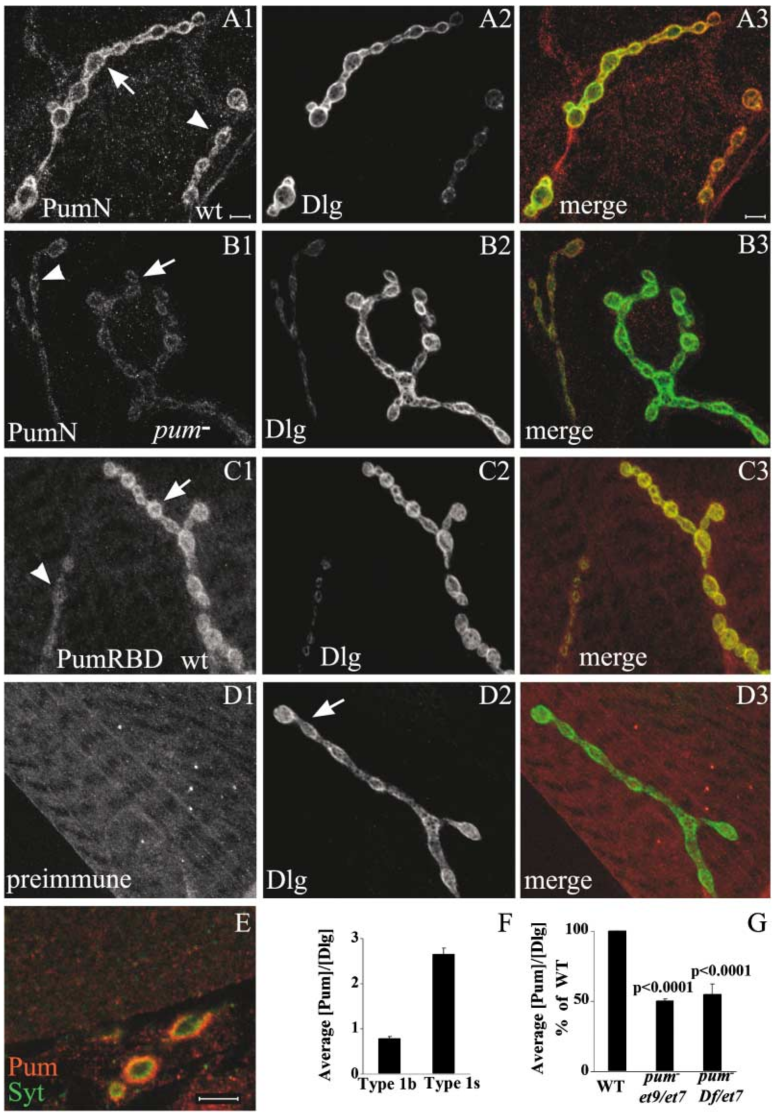

Figure 2. Pumilio Is Localized to the Postsynaptic Side of the NMJ

The NMJ region of muscle 4 is shown in all panels, stained with fluorescent antibodies and visualized with confocal microscopy. All panels are z series projections except (E), which is a single confocal slice. In the first four rows, the first panel shows anti-Pum (or control preimmune serum [D1]) staining, the second panel shows staining for Dlg, a postsynaptic marker, and the third panel (color) is a merge of the two images. Type Ib boutons, arrows; Type Is boutons, arrowheads. (A1–A3) Wild-type (*w^{1118}*; labeled as wt), double stained with anti-PumN (rabbit; red) and anti-Dlg (mouse; green). Pum colocalizes with Dlg at all NMJ boutons, and Ib and Is boutons stain with similar intensity. There is much less Dlg at Is boutons, so the ratio of Pum to Dlg staining is higher on Is boutons than on Ib boutons. (B1–B3) *pum^{ET9}/pum^{ET7}* (labeled as *pum^{-}*) double stained with anti-PumN (red) and anti-Dlg (green). Pum staining is much weaker than in wild-type (compare [B1] and [A1]). As a result, the Ib boutons in (B3) are greener than those in (A3), and the Is boutons are fainter. Panel sets (A) and (B) were imaged at the same time with identical settings on the confocal microscope. (C1–C3) Wild-type (*w^{1118}*; labeled as wt), double stained with anti-PumRBD (rat; red) and anti-Dlg (green). Pum colocalizes with Dlg at all NMJ boutons. With this antibody, however, Ib boutons stain more brightly than Is boutons. (D1–D3) Wild-type (*w^{1118}*), double stained with rabbit preimmune serum (red) and anti-Dlg (green). In these panels, the threshold for displayed intensity has been lowered to clearly show background staining. In (D1), the muscle fiber's striations can be seen, but the NMJ is not visible. Scale bar in (A3) (5 μm) applies to all panels in (A)–(D). (E) High-magnification view of three muscle 4 type Ib boutons in *w^{1118}*, stained with anti-PumRBD (red) and anti-Syt (green). Syt is exclusively presynaptic. Red Pum staining surrounds green Syt staining, and there is little overlap between them. Scale bar, 5 μm. (F) A bar graph of the intensity ratio between anti-PumN and anti-Dlg staining in *w^{1118}* NMJs at type Ib and Is boutons, for NMJs on several different muscles (muscles 4, 6/7, 12, and 13 and five to seven boutons of each type per NMJ). The Pum/Dlg ratio is about 3-fold higher at Is boutons (2.65 ± 0.13; n = 30 NMJs) than at Ib boutons (0.78 ± 0.04; n = 43 NMJs). The standard errors are indicated above the bars. (G) A bar graph of the Pum/Dlg ratio (in percent of wild-type) at Is boutons of wild-type (*w^{1118}*; labeled as wt), *pum^{ET9}/pum^{ET7}* (labeled as *pum^{-} et9/et7*), and *pum^{ET7}/Df(3R)BSC24* (labeled as *pum^{-}Df/et7*). The actual percentages are 50.1 ± 1.5 for *pum^{ET9}/pum^{ET7}* (n = 32 NMJs, five to seven boutons per NMJ) and 54.9 ± 7.3 for *pum^{ET7}/Df(3R)BSC24* (n = 7 NMJs, five to seven boutons per NMJ). Standard errors are indicated above the bars. The differences between wild-type (*w^{1118}*; labeled as WT) and both *pum* mutant genotypes are highly significant ($p < 0.0001$; Student's t test).

Figures 2B1–2B3 show double staining of muscle 4 NMJs in a *pum^{ET9}/pum^{ET7}* larva. Pum staining is much weaker than in wild-type (compare Figure 2B1 to Figure 2A1), indicating that the NMJ staining observed in wild-type represents authentic Pum protein. We also stained *pum^{ET7}/Df(3R)BSC24* larvae and obtained similar results. We then measured the fluorescence intensity of Pum and Dlg at Ib and Is boutons (five to seven boutons of each type per NMJ) of many NMJs in three genotypes: wild-type (30 NMJs), *pum^{ET9}/pum^{ET7}* (32 NMJs), and *pum^{ET7}/Df(3R)BSC24* (7 NMJs). Pum staining intensity is higher relative to Dlg at Is boutons (Figure 2F). In *pum^{ET9}/pum^{ET7}* and *pum^{ET7}/Df(3R)BSC24* larvae, the Pum/Dlg fluorescence intensity ratio is reduced by a factor of about 2 relative to wild-type at Is boutons (Student's t test; $p < 0.0001$ for both *pum^{ET9}/pum^{ET7}* and *pum^{ET7}/Df(3R)BSC24*; Figure 2G).

Anti-PumRBD also specifically stains NMJs in wild-type larvae (Figure 2C). With this antibody, Ib boutons stain more strongly than Is boutons (Figure 2C1), and the reduction in staining in mutants is less dramatic than that with anti-PumN (data not shown). For additional controls, we double stained larvae with preimmune rabbit or rat serum and anti-Dlg and lowered the intensity cutoff in order to display background staining (Figure 2D). These panels show that under conditions where nonspecific staining of the muscle fiber is clearly visible (Figure 2D1), there is no detectable staining of NMJs over background. Other larval NMJs, as well as adult abdominal NMJs, also stain with anti-Pum (Supplemental Figure S1 at http://www.neuron.org/cgi/content/full/44/4/663/DC1/).

To further define the localization of Pum at the NMJ, we double stained larvae with anti-Pum and a variety of other presynaptic markers. Figure 2E shows a single confocal section of muscle 4 NMJ Ib boutons stained with anti-PumRBD and anti-Synaptotagmin (Syt). Syt, a synaptic vesicle protein, is exclusively presynaptic. It is localized to the bouton borders and to puncta within these borders. Red Pum staining forms rings around the green Syt staining at each bouton, and there is little overlap between red and green, indicating that Pum is primarily postsynaptic at the NMJ. We obtained similar results by double staining for Pum and two other presynaptic markers, cysteine string protein and the epitope recognized by anti-horseradish peroxidase antibodies (data not shown).

To analyze the Pum proteins made in wild-type and mutant muscles, we examined larval body wall lysates by Western blotting with anti-PumN. We found that body wall lysates from wild-type larvae contain three Pum proteins with apparent molecular weights of approximately 156, 130, and 93 kilodaltons (kD), consistent with results reported with adult fly heads and ovaries (Parisi and Lin, 1999; Schweers et al., 2002). In lysates from *pum*^{ET9}/*pum*^{ET7} mutants, the amounts of the two larger isoforms are greatly reduced, but the intensity of band(s) migrating at 93 kDa is greater than in wild-type (Supplemental Figure S2 at http://www.neuron.org/cgi/content/full/44/4/663/DC1/).

Pumilio Regulates NMJ Morphology

To analyze synaptic morphology, wild-type control (*w*^{1118}) and *pum* mutant NMJs in third instar larvae were stained with anti-Syt to visualize synaptic boutons and with monoclonal antibody (mAb) 1D4 against Fasciclin II to visualize NMJs and axons. Figure 3A shows anti-Syt staining of a wild-type NMJ on muscle 12. The *pum*^{ET9}/*pum*^{ET7} muscle 12 Ib NMJ shown in Figure 3B differs in a number of ways from wild-type. First, the synaptic span (the largest distance between the terminal boutons of the Ib synapse) is much smaller in *pum* mutants. Second, abnormally large boutons are seen in *pum* mutant Ib NMJs (arrowhead). Third, the total number of Ib boutons is reduced in *pum* NMJs. Similar phenotypes were observed in Fasciclin II-stained preparations (Figures 3E and 3F). This phenotype suggests that individual boutons may have failed to separate from each other during bouton division.

To quantify the observed phenotypes, we measured the areas occupied by the three terminal boutons of many type Ib synaptic branches within muscle 12 NMJs (see the Supplemental Data at http://www.neuron.org/cgi/content/full/44/4/663/DC1/). As shown in Figure 3J, the average area of a type Ib bouton is increased by a factor of more than 2 in *pum*^{ET9}/*pum*^{ET7} mutants. This increase in size is accompanied by a 1.8-fold decrease in the total number of type Ib boutons per NMJ (Figure 3K). Ib NMJs on other muscles were affected in a similar manner (data not shown).

The phenotypes documented here for *pum*^{ET9}/*pum*^{ET7} mutants are highly significant ($p < 0.0001$). *pum*^{Msc}/*pum*^{ET7} mutants had similar but less penetrant phenotypes, while no defects were seen in *pum*^{ET9}/+ heterozygote larvae (see Figure 3 legend). To determine the causes of the NMJ phenotypes seen in *pum* LOF mutants, we combined the *pum*^{ET9} and *pum*^{ET7} mutations with UAS-*pum* cDNA transgenic lines and with neuronal and muscle GAL4 drivers. The UAS constructs encoded either full-length Pum or its C-terminal PUF RBD region (aa 1093–1533). The PUF RBD has been shown to be sufficient for rescue of maternal *pum* phenotypes in the early embryo (Wharton et al., 1998). High-level GAL4-driven expression of full-length Pum in neurons or muscles produced lethality. However, we were able to define conditions under which we could express Pum at lower levels in either tissue and obtain viable larvae (see the Supplemental Data at http://www.neuron.org/cgi/content/full/44/4/663/DC1/for details).

We found that neuronal expression of full-length Pum is sufficient to rescue the defects in Ib NMJ morphology seen in *pum* mutants. To assay rescue, we expressed full-length Pum or the Pum RBD in the *pum*^{ET9}/*pum*^{ET7} mutant background, driving expression at 18°C either in postmitotic neurons (with Elav-GAL4) or in muscles (by "leaky" expression from MHC-GS-GAL4 in the absence of steroid) (Osterwalder et al., 2001; Roman et al., 2001). Full-length Pum expression in neurons rescued the synaptic morphology phenotypes (Figures 3C, 3G, 3J, and 3K), while expression in muscles had no effect (Figures 3D and 3K). Both the average size and the number of type Ib boutons on muscle 12 were restored to wild-type by neuronal Pum expression (Figures 3J and 3K). Pum RBD expression in neurons did not rescue the mutant phenotype, in contrast to its ability to provide the early abdominal segmentation function (Figure 3K) (Wharton et al., 1998).

The morphology of Is boutons was not obviously altered in *pum* mutants, and their numbers were increased. This Is phenotype is due to loss of postsynaptic Pum and is discussed below.

Pumilio Overexpression Produces a Phenotype with More Numerous and Smaller Boutons

Having observed that loss of *pum* function in neurons produces a phenotype with larger and fewer type Ib NMJ boutons, we wondered whether neuronal overexpression of Pum would also have an effect on NMJ morphology. To investigate this, we stained escaper larvae from crosses of UAS-full-length Pum to Elav-GAL4 conducted at 29°C with anti-FasII or anti-Syt. Muscle 12 NMJs in these Pum-overexpressing larvae had much smaller boutons than controls (*w*^{1118} × Elav-GAL4 at 29°C) (Figures 3H and 3I). The average number of type Ib boutons (identified by Dlg staining; see the Supplemental Data at http://www.neuron.org/cgi/content/full/44/4/663/DC1/) on muscle 12 was approximately 3-fold higher in overexpression larvae relative to controls (Figure 3K, right). Similar phenotypes were observed at other NMJs. Pum RBD overexpression had no effect. Thus, overexpression and loss of Pum in neurons generate opposite phenotypes.

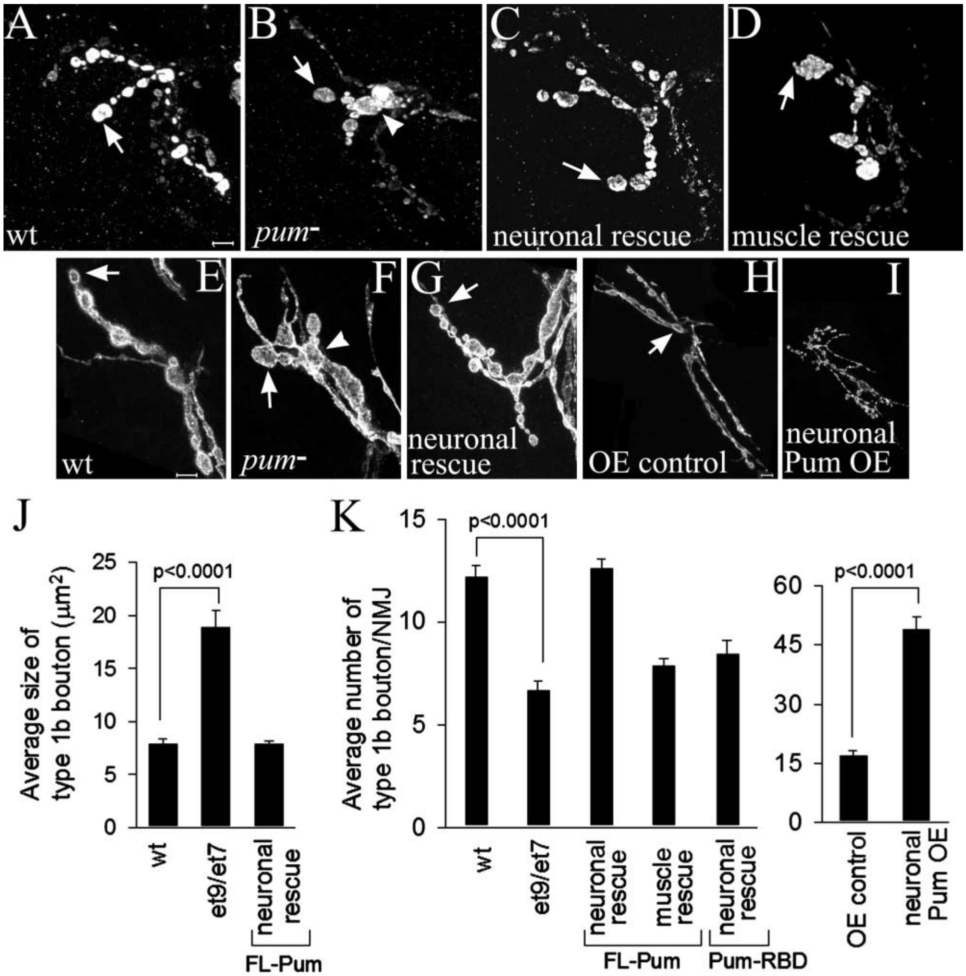

Figure 3. *pumilio* Mutant and Neuronal Overexpression Larvae Have Altered NMJ Morphologies

NMJs on muscle 12 are shown in all panels, labeled either with anti-Syt (A–D) or with anti-FasII (mAb 1D4; [E]–[I]). (A–G) Loss of function and rescue. (A and E) Wild-type (labeled as wt, w^{1118}); (B and F) pum^{ET9}/pum^{ET7} (labeled as pum^{-}); (C and G) neuronal Pum rescue (labeled as neuronal rescue; genotype *Elav-GAL4; pum*^{ET9}/ *UAS-pum, pum*^{ET7}); (D) muscle Pum rescue (labeled as muscle rescue; genotype *MHC-GSGAL4, pum*^{ET9}/*UAS-pum, pum*^{ET7}). Arrows indicate a terminal type Ib bouton in all panels; arrowheads in (B) and (E) indicate abnormal large central boutons with a fused appearance. (H and I) Neuronal Pum overexpression. NMJs on muscle 12 (at a lower magnification to show the whole NMJ) from control (genotype *Elav-Gal4* crossed to w^{1118}; labeled as wt in [H]) and neuronal Pum overexpression (genotype *Elav-GAL4/UAS-full length Pum*; labeled as neuronal Pum-OE in [I]) larvae are shown. Arrows indicate type Ib boutons in the NMJs from control larvae. A2 hemisegments are shown in all panels. Scale bar in (A) is 5 μm and applies to (A)–(G); scale bar in (H) is 5 μm and applies to (H) and (I). (J) Type Ib boutons are increased in size in *pum* mutants. Graph of the average bouton size (units μm^2) of three terminal type Ib boutons on muscle 12 synapses in w^{1118} (wt; n = 26), pum^{ET9}/pum^{ET7} (*et9/et7*; n = 20), and neuronal Pum rescue larvae (neuronal rescue with FL-Pum; n = 46). Neuronal rescue restores the average bouton size to the wild-type value. The difference between the average bouton sizes in pum^{ET9}/pum^{ET7} and wild-type is highly significant ($p < 0.0001$; Student's t test). Bouton size in $pum^{ET9}/+$ larvae was 7.92 ± 0.46 (n = 6), not significantly different from wild-type. In all three graphs (J and K), A2 hemisegments were analyzed. Muscle sizes for all genotypes did not differ significantly from wild-type. Standard errors are indicated above each bar. (K) *pum* mutants have a reduced number of Ib boutons (left), and Pum neuronal overexpression larvae have an increased number (right). (Left) Graph of the average number of type Ib boutons on muscle 12 synapses in w^{1118} (wt; n = 33), pum^{ET9}/pum^{ET7} mutants (*et9/et7*; n = 29), neuronal Pum rescue larvae (neuronal rescue with FL-Pum; n = 47), muscle Pum rescue larvae (muscle rescue with FL-Pum; n = 18), and neuronal PumRBD rescue larvae (*Elav-GAL4; pum*^{ET9}/ *UAS-pumRBD, pum*^{ET7}; neuronal rescue with PumRBD; n = 8). The difference between the average Ib bouton numbers in pum^{ET9}/pum^{ET7} and w^{1118} is highly significant ($p < 0.0001$; Student's t test). (Right) Graph of type Ib bouton numbers in overexpression (OE) control (n = 7) and neuronal Pum overexpression (labeled as neuronal Pum OE; n = 6) larvae. The difference between the average bouton numbers in control and Pum overexpression larvae is highly significant ($p < 0.0001$; Student's t test).

Postsynaptic Accumulation of the Translation Factor eIF-4E in *pumilio* Mutants

Pum is expressed in the cytoplasm in neurons (Figure 1), and the synaptic morphology defects in Ib boutons seen in LOF mutants are rescued by neuronal Pum expression (Figure 3). These findings on neuronal Pum thus do not define the functions of Pum at the NMJ, where it appears to be postsynaptically localized within the muscle fiber (Figure 2). Since Pum acts as a translational repressor during early development, we thought that it might be involved in local regulation of mRNA translation or mRNA stability in the postsynaptic SSR

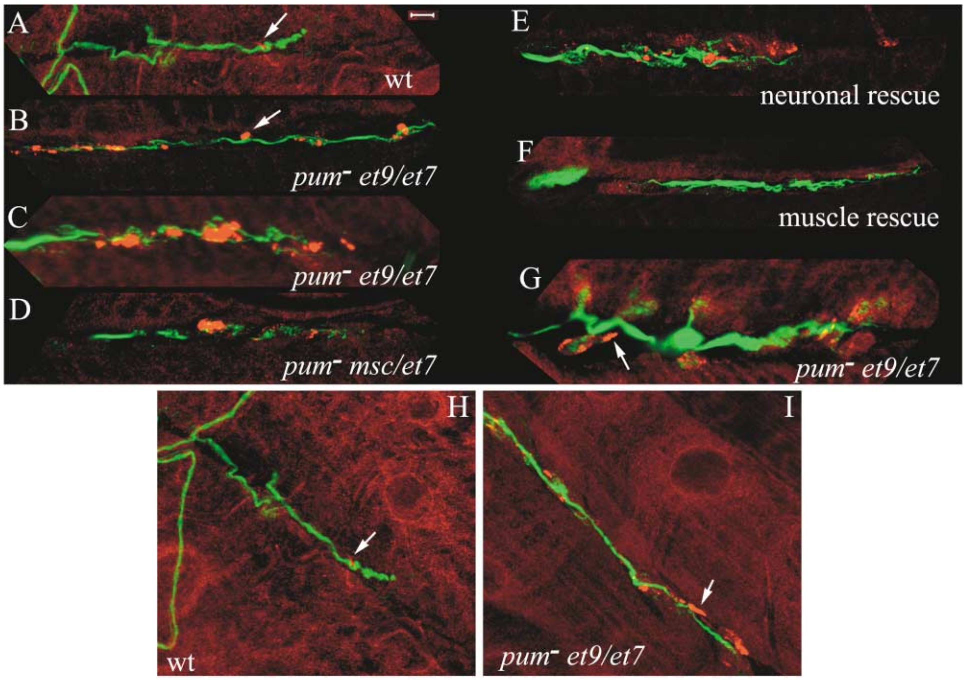

Figure 4. eIF-4E Aggregates at NMJs Are Increased in Number in *pumilio* Mutant Larvae

Larval fillets were stained with anti-eIF-4E (red) and anti-Futsch (green); the NMJ at the cleft between muscles 6 and 7 is shown in all panels. (A and H) wild-type (w^{1118}; labeled as wt); (B, C, G, and I) pum^{ET9}/pum^{ET7} (labeled as pum^{-} *et9/et7*); (D) pum^{Msc}/pum^{ET7} (labeled as pum^{-} *msc/et7*); (E) neuronal Pum rescue (genotype *Elav-GAL4;* pum^{ET9}/ *UAS-pum,* pum^{ET7}); (F) muscle Pum rescue (genotype *MHC-GSGAL4,* pum^{ET9}/ *UAS-pum-tub 3′UTR,* pum^{ET7}). (A)–(F), (H), and (I) are confocal z series projections; (G) is a single confocal slice through the NMJ. In (H) and (I), eIF-4E staining intensity across the muscle fiber is not increased in pum^{ET9}/pum^{ET7}, but the synaptic cleft in the *pum* mutant has several aggregates, while the wild-type has only one. A3 hemisegments are shown in all panels. Arrows indicate aggregates. Scale bar, 5 μm.

that underlies NMJs. Schuster and his colleagues have shown that postsynaptic aggregates of the translation factor eIF-4E can be visualized at NMJs, especially under conditions where larvae are induced to move vigorously (Sigrist et al., 2000, 2003).

To evaluate the effects of *pum* mutations on postsynaptic eIF-4E accumulation, we visualized eIF-4E aggregates in various genotypes by staining larvae with antibodies against eIF-4E and Futsch (a presynaptic microtubule marker) after induction of movement (Sigrist et al., 2003; see the Supplemental Data at http://www.neuron.org/cgi/content/full/44/4/663/DC1/) (Figure 4). We counted the number of eIF-4E aggregates at muscle 6/7 NMJs in segments A2–A5 (Sigrist et al., 2000, 2003), and these data are displayed in Figure 5A.

In two wild-type reference strains, w^{1118} and *Oregon R* (*OR*), 2.1 and 4.8 eIF-4E aggregates per NMJ, respectively, were observed after induction of movement, consistent with earlier findings (Sigrist et al., 2000, 2003) (Figures 4A and 5A; see the Supplemental Data at http://www.neuron.org/cgi/content/full/44/4/663/DC1/). In *pum* mutants, we observed large increases in the number of eIF-4E aggregates relative to these controls. For pum^{ET9}/pum^{ET7} larvae, we counted a total of 2001 aggregates among 80 NMJs, or 25 aggregates per NMJ (Figures 4B, 4C, 4G, and 5A). This represents a 5- to 12-fold increase in the number of aggregates per NMJ relative to the two wild-type controls. pum^{Msc}/pum^{ET7} larvae also had a large number of aggregates (18 per NMJ) (Figures 4D and 5A). Many eIF-4E aggregates were also observed at muscle 12 and other NMJs in both *pum* genotypes (data not shown). Aggregate numbers in $pum^{ET9}/+$ heterozygote larvae did not differ significantly from wild-type (4.6 per NMJ; Figure 5A).

eIF-4E aggregates are of various sizes and intensities and therefore contain different amounts of eIF-4E. To obtain an estimate of the relative amounts of eIF-4E contained within synaptic aggregates at NMJs in the different genotypes, we also determined the number of pixels occupied by each aggregate and the intensity of these pixels. The average amount of eIF-4E per NMJ was calculated from these data. We found that pum^{ET9}/pum^{ET7} larvae had 5.4- to 12-fold more eIF-4E per muscle 6/7 NMJ than the wild-type controls (Figure 5B), consistent with the conclusions obtained from the aggregate counts (see the Supplemental Data at http://www.neuron.org/cgi/content/full/44/4/663/DC1/).

Figures 4A–4F are confocal z series projections that allow all of the eIF-4E aggregates at a muscle 6/7 NMJ to be visualized. Figure 4G is a single confocal slice of a *pum* mutant NMJ, showing that eIF-4E aggregates are in the same focal plane as the presynaptic elements defined by Futsch staining. Since eIF-4E is an essential translation factor that is encoded by a single gene in *Drosophila* and is therefore expressed in all cells, we needed to evaluate whether the effects of *pum* mutations on muscle eIF-4E were restricted to the NMJ region. To do this, we examined confocal projections over the entire muscle surfaces, so that we could determine if the levels of eIF-4E in the surrounding muscle fibers

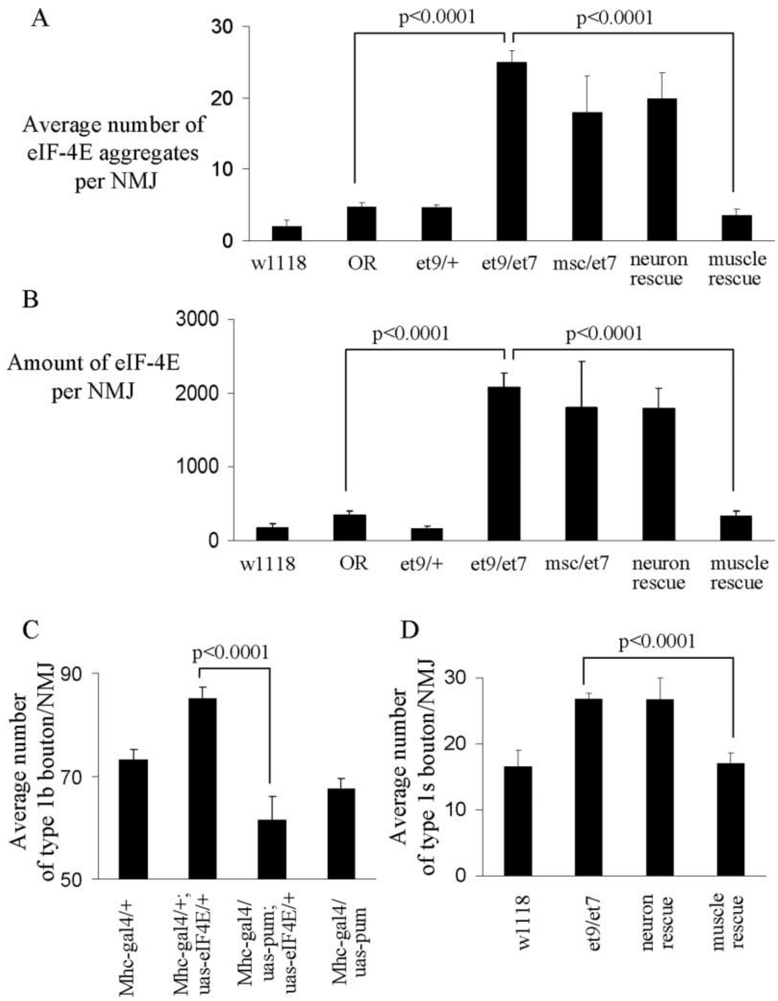

Figure 5. Effects of Loss and Gain of Postsynaptic Pumilio: Quantitation of eIF-4E, Suppression of eIF-4E-Induced Increases in Ib Bouton Number, and Changes in Is Bouton Number

(A) eIF-4E aggregate counts. A bar graph of the average numbers of eIF-4E aggregates at the muscle 6/7 NMJ (segments A2–A5) in various genotypes. Larvae were fixed 3 hr after transfer from liquid food to solid medium to induce movement. (B) Amounts of eIF-4E in NMJ aggregates. A bar graph of the average amount of eIF-4E at the muscle 6/7 NMJ, calculated by multiplying the average pixel intensity by the area of each aggregate and summing the values for the aggregates at each NMJ. The genotypes and conditions are the same as for the graph in (A). (C) Genetic interactions between *pum* and *eIF-4E*. A bar graph of the number of type Ib boutons on muscle 6/7 NMJs in control larvae (genotype *MHC-Gal4/+*; n = 14), larvae overexpressing eIF-4E only (genotype *MHC-Gal4/+;UAS-eIF-4E/+*; n = 22), larvae overexpressing both eIF-4E and full-length Pum (genotype *MHC-Gal4/UAS-pum-tub-3′UTR;UAS-eIF-4E/+*; n = 7), and larvae overexpressing Pum only (genotype *MHC-Gal4/UAS-pum-tub-3′UTR*; n = 20). A2 hemisegments were scored. (D) Is bouton phenotype in *pum* mutants is rescued by muscle Pum expression. A bar graph of the number of type Is boutons on muscle 4 is shown. Standard errors are indicated above the bars, and the significances of the differences between genotypes (Student's t test) are indicated above the brackets connecting the relevant bars. Genotype information and raw data for this figure are in the Supplemental Data at http://www.neuron.org/cgi/content/full/44/4/663/DC1/.

were changed. As shown in Figures 4H and 4I, there were no apparent increases in the levels of eIF-4E across muscle fibers 6 and 7 in *pum* mutants as compared to controls (w^{1118}).

The increase in synaptic eIF-4E aggregates in *pum* mutants is due to the loss of Pum expression on the postsynaptic side of the NMJ. This was demonstrated by expressing Pum in muscles or in neurons of pum^{ET9}/pum^{ET7} larvae as described above. Expression of Pum in muscles of pum^{ET9}/pum^{ET7} mutants reduced the number of eIF-4E aggregates by 7-fold, to 3.5 aggregates per NMJ (Figures 4F and 5A). These numbers are between the values obtained for the two wild-type controls, indicating that rescue was essentially complete. Similarly, calculation of the amounts of eIF-4E at NMJs showed that muscle expression of Pum reduced eIF-4E levels by 6.5-fold (Figure 5B). In contrast, neuronal expression of Pum in pum^{ET9}/pum^{ET7} larvae did not greatly decrease the number of eIF-4E aggregates (to 19.9 aggregates per NMJ, a 20% reduction; Figures 4E and 5A). Levels of eIF-4E were 88% of those in pum^{ET9}/pum^{ET7} (Figure 5B).

In our experiments, eIF-4E aggregates were rarely seen in wild-type larvae unless they were induced to move by transfer to solid media. If Pum is essential for repression of postsynaptic eIF-4E accumulation in less motile larvae maintained in liquid slurry food (Sigrist et al., 2003; see the Supplemental Data at http://www.neuron.org/cgi/content/full/44/4/663/DC1/), one might expect that high levels of eIF-4E would be observed at the NMJs of *pum* LOF mutant larvae even when they were not induced to move. In fact, we found that pum^{ET9}/pum^{ET7} mutants picked directly from liquid food had large numbers of eIF-4E aggregates (15.5 aggregates per NMJ) and had eIF-4E levels that were only 36% lower than larvae from the same vial that were induced to move. These results imply that in the absence of Pum, postsynaptic eIF-4E expression is derepressed even without induction of movement.

Genetic Interactions between *pumilio* and *eIF-4E*

When eIF-4E expression is artificially elevated in muscles, the number of NMJ boutons is increased, perhaps because new active zones are recruited to glutamate receptor clusters that accumulate at sites of postsynaptic translation (Sigrist et al., 2000). If Pum is a limiting component of the normal mechanisms by which eIF-4E expression is controlled, elevation of Pum levels in muscle should suppress the phenotypic effects of eIF-4E overexpression.

To test this, we found an MHC-GAL4 insertion that allows survival of *F1* larvae after crossing to UAS-full-length Pum at 25°C. These Pum-overexpressing larvae displayed no significant change in Ib bouton numbers relative to controls (Figure 5C). To overexpress eIF-4E, we crossed this same driver line to the UAS-eIF-4E line employed by Sigrist et al. (2000). This produced an increase in the number of type Ib boutons on muscle 6/7 as compared to the control (Ib bouton number in MHC-GAL4; UAS-eIF-4E = 85.1; control MHC-GAL4/+ = 73.3; $p < 0.001$; Student's t test; Figure 5C). This increase is smaller than that reported by Sigrist et al. (2000) but is still significant.

To test the effect of Pum on the *eIF-4E* gain-of-function phenotype, we simultaneously expressed full-length Pum and eIF-4E in muscles using this driver and counted Ib boutons on muscle 6/7. We observed that the increase in Ib bouton number conferred by overexpressing eIF-4E in muscle was completely suppressed by also overexpressing Pum (Ib bouton number in MHC-Gal4/UAS-Pum, UAS-eIF-4E = 61.4, versus 85.1 in MHC-Gal4; UAS-eIF-4E; $p < 0.0001$; Student's t test). Ib bouton numbers in larvae overexpressing both eIF-4E and Pum were not significantly different from those in larvae overexpressing only Pum (Figure 5C).

Because driving eIF-4E overexpression in muscles increases bouton number (Sigrist et al., 2000; Figure 5C), and postsynaptic eIF-4E levels are elevated in *pum* mutants (Figure 5B), one might have expected that loss of Pum would also increase bouton number. In Figure 3, we showed that Ib bouton numbers are reduced in *pum* mutants. This is a presynaptic effect, because it is rescued by expression of Pum in neurons. In contrast, Is boutons were increased in number by about 1.7-fold in *pum* mutants (27.4 ± 1.86 in pum^{ET9}/pum^{ET7} versus 16.6 ± 2.4 in w^{1118}). This phenotype is due to loss of postsynaptic Pum, because it is fully rescued by expressing Pum in muscles and unaffected by Pum expression in neurons (Figure 5D). The increase in Is bouton number could be due to derepression of eIF-4E and the consequent accumulation of glutamate receptor clusters that recruit new active zones (see below).

Pumilio Binds Directly to the 3′UTR of *eIF-4E* mRNA

Having observed that eIF-4E levels at the NMJ are greatly increased in *pum* mutants, we wondered whether *eIF-4E* mRNA might be a direct Pum target. Functional Pum binding sites (NREs) have thus far been defined only in *hb* and *bcd* mRNAs (Wharton et al., 1998).

To determine whether Pum can bind to the *eIF-4E* 3′UTR, we performed binding experiments with a GST-Pum RBD fusion protein used previously to characterize interactions with the *hb* NRE (Wharton et al., 1998; Zamore et al., 1999) and two different fragments of the *eIF-4E* 3′UTR. Pum binds as tightly to nucleotides (nt) 131–252 of the *eIF-4E* 3′UTR as it does to the *hb* NRE (Figure 6). In contrast, nt 1–130 of the *eIF-4E* 3′UTR do not bind selectively to Pum. Binding to nt 1–130 is as weak as to a *hb* NRE with a double point mutation in a critical binding element (Wharton et al., 1998). Thus, Pum appears to bind with high affinity and specificity to the 3′ half of the *eIF-4E* mRNA.

We then tested binding to subfragments of the 3′ half of the *eIF-4E* 3′UTR and found that a 51 nt RNA (nt 161–212) bound as tightly as the entire sequence (data not shown). To further characterize the specificity of this binding, we performed competition experiments, in which unlabeled wild-type *hb* NRE or the double point mutant *hb* NRE RNAs were used to compete binding by labeled *eIF-4E* RNAs. Figure 6C shows such a competition experiment, using a 69 nt *eIF*-4E RNA (nt 161–230) and the intact Pum RBD (not fused to GST). Binding to this RNA is efficiently competed by wild-type *hb* NRE RNA but not by the mutant RNA, further indicating that binding to *eIF-4E* 3′UTR sequences is specific. Similar results were obtained in competition experiments with the 51 nt RNA and other 3′UTR fragments (data not shown).

The *eIF-4E* 3′UTR sequences from *Drosophila melanogaster* and *Drosophila pseudoobscura* display significant similarity. The 51 nt Pum binding RNA sequence has a 24/51 match (one gap) between the two species (Figure 6D). However, this sequence is not obviously related to that of the *hb* NRE. There are two UGU triplets, which are critical for Pum binding to *hb* sequences (Wharton et al., 1998) within the 51 nt sequence, but mutating either or both of these triplets did not strongly affect Pum binding affinity (data not shown). Thus, the Pum binding sites in *eIF-4E* mRNA, like those in *CycB* mRNAs (L. Kadyrova, Y.H., and R.P.W., unpublished data) appear to be different from the characterized sites in *hb* and *bcd* mRNAs.

The GluRIIa Glutamate Receptor Is Upregulated in *pumilio* Mutants

eIF-4E levels are normally limiting for translation (Sonenberg and Gingras, 1998), and postsynaptic eIF-4E is increased in *pum* mutants (Figures 4 and 5). mRNA encoding the ionotropic glutamate receptor GluRIIa is localized to the synaptic region of the muscle (Sigrist et al., 2000), suggesting that this mRNA might be a target for postsynaptic translational control. We therefore examined whether the levels of this receptor are changed at *pum* mutant NMJs.

Figure 7A shows double staining of a wild-type muscle 12 NMJ with anti-GluRIIa (red) and anti-Syt (green). Only a few red GluRIIa puncta are visible around the Ib boutons, which stain brightly with anti-Syt (arrow). Higher densities of dim GluRIIa dots are seen at the Is boutons, which have only weak anti-Syt staining (arrowhead). A similar pattern of staining is seen at the muscle 4 synapse (Figure 7B).

GluRIIa expression is dramatically changed in pum^{ET9}/pum^{ET7} and pum^{ET7}/*Df(3R)BSC24* mutants. Staining is much brighter and puncta are more numerous at muscle 12, muscle 4, and muscle 6/7 NMJs (Figures 7C–7F). This is particularly obvious for Is boutons (arrowheads in Figures 7C and 7D). We also examined expression of GluRIIB and GluRIII (Marrus et al., 2004; Petersen et al., 1997) in *pum* mutants and observed no change from the levels seen in wild-type (data not shown).

The Frequency of Spontaneous Neurotransmitter Release Is Increased in *pumilio* Mutants

Figure 8 shows the responses to evoked transmitter release (excitatory evoked junctional potential [EJP] amplitude), quantal content, and two measures of sponta-

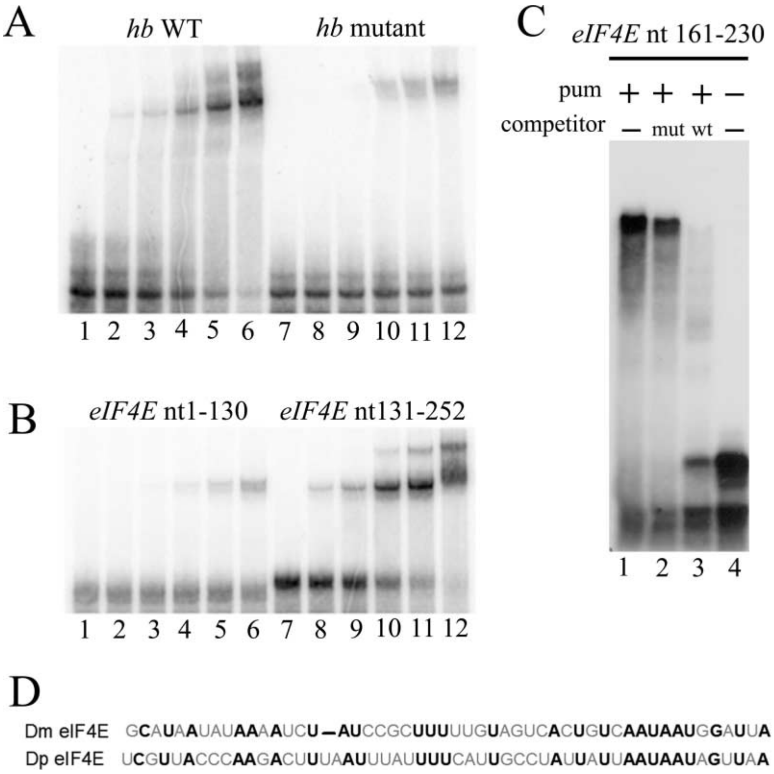

Figure 6. Pumilio Binds Selectively to the 3′UTR of *eIF-4E* mRNA

Electrophoretic mobility shift assays were performed with the Pumilio RNA binding domain fused to GST (A and B) or the unfused, intact RBD (C) and *hunchback* (*hb*) 3′UTR NRE (A) and *eIF-4E* 3′UTR RNAs (B and C), as described by Wharton et al. (1998). (A) Lanes 1–6 are binding reactions with the wild-type *hb* NRE; lanes 7–12 are binding reactions with the UG21AC mutant *hb* NRE. (B) Lanes 1–6 are binding reactions with nt 1–130 of the *eIF-4E* 3′UTR; lanes 7–12 are binding reactions with nt 131–252 of the *eIF-4E* 3′UTR. For lanes 1–6 of each panel, 10 μl reactions contained 0, 10, 30, 100, 300, or 1000 ng, respectively, of GST-Pum fusion. Note that half-maximal binding to the wild-type *hb* and *eIF-4E* (131–252) sequences occurs at approximately the same concentration of Pum protein. (C) A competition experiment in which binding of Pum-RBD (500 ng) to a labeled 69 nt *eIF-4E* RNA (nt 161–230) is competed by 150 ng of unlabeled wild-type *hb* NRE RNA (WT) or a double mutant UG21AC *hb* NRE RNA (mut). Note that the Pum:RNA complex band is eliminated by inclusion of WT RNA competitor, but there is only a moderate reduction in its intensity when mutant RNA is used as competitor. (D) Alignment of the minimal 51 nt *eIF-4E* 3′UTR binding sequence in *D. melanogaster* (*Dm*) to *D. pseudoobscura* (*Dp*) sequence. Conserved residues are in bold; a gap has been introduced to optimize the alignment.

neous release (mini-EJP [mEJP] amplitude and frequency) obtained from various genotypes. There is no consistent change in the evoked response relative to wild-type in *pum* mutants. Quantal content in the strongest *pum* mutant genotypes (pum^{ET9}/pum^{ET7} and $pum^{ET7}/Df(3R)BSC24$) is reduced due to their elevated mEJP amplitudes (black bars in Figure 8C; QC = EJP amplitude/mEJP amplitude). However, an increase in mEJP

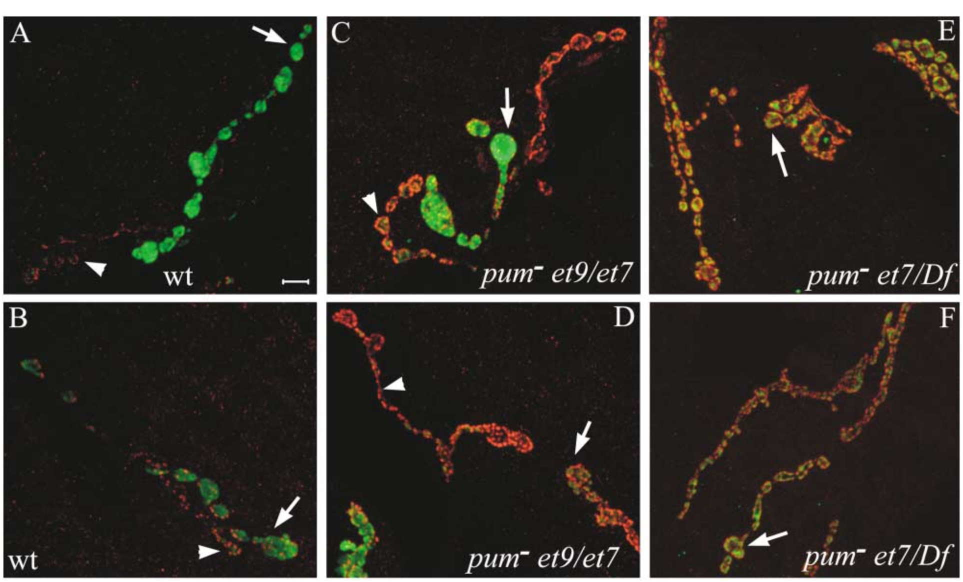

Figure 7. The GluRIIa Receptor Is Upregulated at NMJs in *pumilio* Mutant Larvae

Wild-type (w^{1118}; labeled as wt) (A and B), pum^{ET9}/pum^{ET7} (C and D), and $pum^{ET7}/Df(3R)BSC24$ (E and F) larvae were stained with anti-GluRIIa (red) and anti-Syt (green). NMJs on muscle 12 (A and C), muscle 4 (B, D, and F), and muscle 6/7 (E) are shown. Arrows indicate type Ib boutons (larger, with bright anti-Syt staining); arrowheads indicate type Is boutons (smaller, with weak anti-Syt staining). Note that red staining is much more prominent, and red puncta are more numerous in (C)–(F), especially at Is boutons. Scale bar in (A), 5 μm.

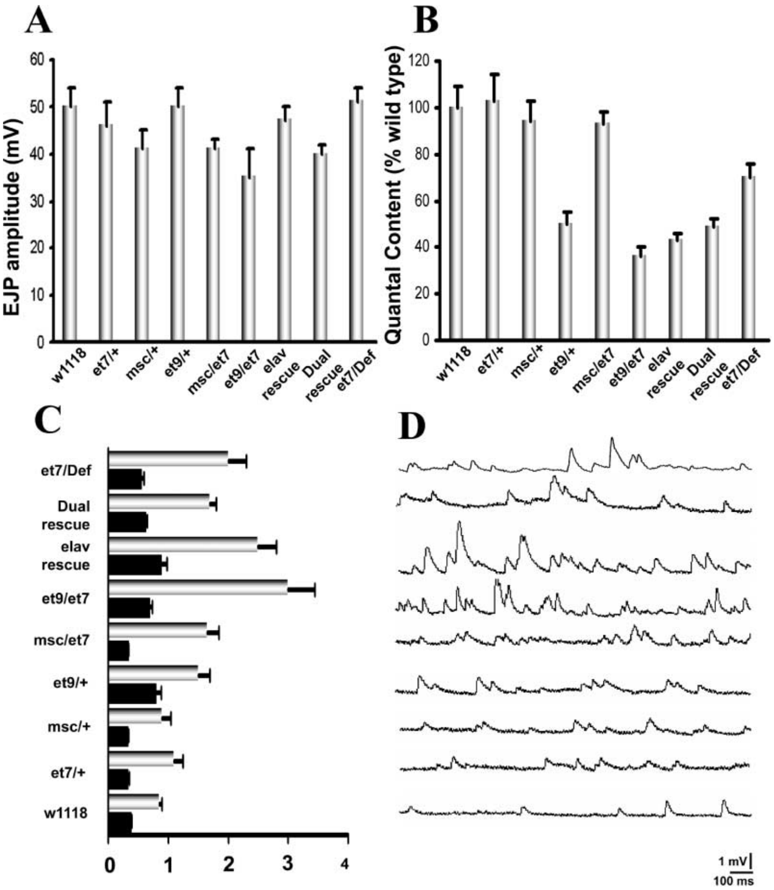

Figure 8. mEJP Frequency Is Increased at *pumilio* Mutant NMJs

(A) Response to evoked transmitter release. The evoked response is somewhat reduced in pum^{ET9}/pum^{ET7} mutants (labeled as et9/et7), but this is not seen in $pum^{ET7}/Df(3R)BSC24$ (et7/Def). (B) Quantal content. This is reduced for all genotypes containing the pum^{ET9} chromosome, because this chromosome appears to produce an elevated mEJP amplitude (see [C]). Neuronal expression of Pum in a pum^{ET9}/pum^{ET7} background (elav rescue) or expression in muscles and neurons in this background (dual rescue) has no effect on quantal content (B) or mEJP amplitude (C) relative to isogenic controls. (C) mEJP frequency (gray bars) and mEJP amplitude (black bars). mEJP frequency is increased in heteroallelic *pum* combinations pum^{ET9}/pum^{ET7}, pum^{Msc}/pum^{Et7} (labeled as msc/et7), and $pum^{ET7}/Df(3R)BSC24$ relative to heterozygotes $pum^{ET9}/+$ (et9/+), $pum^{Msc}/+$ (msc/+), and $pum^{ET7}/+$ (et7/+), and to wild-type (w^{1118}). This phenotype can be rescued to heterozygote levels by combined muscle and neuronal expression of full-length Pum in a pum^{ET9}/pum^{ET7} background (dual rescue). (D) Traces of spontaneous events in the same genotypes reflect these phenotypes. ($n = 9$ for pum^{ET9}/pum^{ET7} and $n = 13$ for dual rescue. For all others, $n = 10$.)

amplitude is not observed for pum^{Msc}/pum^{ET7}, while $pum^{ET9}/+$ larvae do display such an increase. Furthermore, the mEJP amplitude and QC phenotypes of pum^{ET9}/pum^{ET7} are not rescued to near wild-type levels by neuronal, muscle, or dual expression of full-length Pum. Thus, it is unclear whether these phenotypes are due to loss of Pum or to genetic background effects.

The strongest rescuable electrophysiological phenotype that is observed in all *pum* mutant combinations is an increase in the frequency of spontaneous neurotransmitter release (gray bars in Figure 8C, traces in Figure 8D). mEJP frequency is elevated by 1.8- to 3-fold relative to heterozygote and wild-type controls in three different *pum* genotypes (pum^{ET9}/pum^{ET7}, $pum^{ET7}/Df(3R)BSC24$, pum^{Msc}/pum^{ET7}; Figure 8C and 8D). Specifically, the pum^{ET9}/pum^{ET7} mEJP frequency is 200% of $pum^{ET9}/+$ ($p < 0.03$) and 272% of $pum^{ET7}/+$ ($p < 0.01$). Moreover, expression of Pum in both neurons and muscles of pum^{ET9}/pum^{ET7} using dual GAL4 drivers rescues the mEJP frequency to near the level seen in the $pum^{ET9}/+$ heterozygote control (113%; not significantly different from $pum^{ET9}/+$). Taken together, these data indicate that the mEJP frequency phenotype is due to loss of *pum* function.

Discussion

Pumilio is a PUF domain RNA binding protein that represses translation of *hb* mRNA during early embryonic development. In this paper, we demonstrate that Pum has both presynaptic and postsynaptic functions at larval NMJs. Neuronal Pum regulates the morphologies of presynaptic terminals. In its absence, Ib boutons are larger and fewer in number, suggesting that they may have failed to separate from each other during growth of the NMJ. Pum overexpression in neurons produces an opposite phenotype characterized by supernumerary small boutons (Figure 3).

Pum is localized to the postsynaptic side of the NMJ (Figure 2). In *pum* mutants, aggregates of the translation initiation factor eIF-4E accumulate at the NMJ, and this phenotype is rescued by restoring Pum to muscles (Figures 4 and 5). The neurotransmitter receptor GluRIIa is also upregulated (Figure 7). Pum binds selectively to the 3′UTR of *eIF-4E* mRNA, suggesting that this mRNA may be a direct target of Pum regulation (Figure 6).

Pumilio Represses Accumulation of eIF-4E at the NMJ

Pum's postsynaptic localization at the NMJ (Figure 2) suggests that it acts on mRNAs located in the synaptic region of muscle fibers. It could repress local translation of synaptic mRNAs, and this would be consistent with its roles during early development. However, our data are also compatible with models in which Pum regulates mRNA stability, localization, or transport at synapses.

Conceptually, local translation does not seem necessary for synaptic regulation in the *Drosophila* neuromuscular system, since NMJs are often close to muscle nuclei and the strengths of individual synapses within an NMJ branch are not known to be separately controlled. However, Schuster and his colleagues have provided evidence that local translation does occur at the larval NMJ. They suggest that it provides a mechanism to allow rapid assembly of postsynaptic elements under conditions where NMJs need to be strengthened within a short time period (Sigrist et al., 2000, 2002, 2003).

Increasing larval motility produces a rapid increase in synaptic strength at the NMJ and causes the eventual addition of new boutons. These changes are associated with the appearance of eIF-4E aggregates at NMJs (Sigrist et al., 2003). PABP spots are also seen at NMJs, and these appear to colocalize with the eIF-4E aggregates (Sigrist et al., 2000). Aggregate numbers can be elevated genetically by overexpressing eIF-4E in muscles or altering PABP expression. Polysome profiles have been identified in transmission electron micrographs of the SSR, and eIF-4E/PABP aggregates are hypothesized to colocalize with polysomes and thus label sites of postsynaptic translation. However, this has not been directly demonstrated (Sigrist et al., 2000).

The cap binding protein eIF-4E is the limiting factor for translation initiation in many systems (Sonenberg and Gingras, 1998). Thus, the appearance of an eIF-4E aggregate might indicate that sufficient local eIF-4E has accumulated to allow efficient translation at that site. *GluRIIa* mRNA is localized to the NMJ region (Sigrist et al., 2000), and GluRIIa receptor-containing puncta increase in number and intensity under conditions that induce appearance of translational aggregates (Sigrist et al., 2003). This accumulation of GluRIIa may be a consequence of local translation of synaptic *GluRIIa* mRNA.

We showed that Pum represses eIF-4E accumulation at synapses by staining LOF mutants with anti-eIF-4E antibody. In *pum* larvae in which movement had been induced, we saw large increases (5- to 12-fold) in the number of synaptic eIF-4E NMJ aggregates relative to two wild-type reference strains. The amount of eIF-4E in aggregates at each NMJ (evaluated by quantitating aggregate areas and fluorescence intensities) was also elevated by 5- to 12-fold. These phenotypes were fully rescued by restoring Pum expression in muscles (Figures 4 and 5). Genetic manipulations performed by others, such as altering the levels of PABP or eIF-4E or introducing *dunce* mutations, were reported to produce increases of $<$3-fold in the number of eIF-4E aggregates (Sigrist et al., 2000). This suggests that eIF-4E expression may be maximally derepressed when Pum is absent.

Pum is required for repression of eIF-4E accumulation at the NMJ in less motile larvae (those maintained in liquid slurry food), because *pum* mutants have large numbers of eIF-4E aggregates both before and after transfer to solid media and consequent induction of movement. In contrast, manipulation of PABP levels increased eIF-4E aggregate number only after induction of movement (Sigrist et al., 2003). This implies that Pum is upstream of PABP in the control of eIF-4E expression. It is interesting to speculate that the motility-induced appearance of eIF-4E aggregates in wild-type larvae might be due to partial inactivation of Pum in response to motor activity.

Having observed this effect on eIF-4E aggregates in *pum* mutants, we examined Pum binding in vitro to the *eIF-4E* 3′UTR and found that it contains at least one high-affinity site (Figure 6). We defined a 51 nt subfragment that binds selectively to Pum and showed that binding is effectively competed by wild-type *hb* NRE RNAs but not by mutant NREs that do not bind Pum with high affinity. These results indicate that the accumulation of eIF-4E that we observe at the NMJ in *pum* mutants could be caused by an increase in the translational efficiency and/or stability of *eIF-4E* mRNA when it is not bound to Pum. If Pum does repress eIF-4E synthesis, such repression acts selectively on *eIF-4E* mRNA in the postsynaptic region, since eIF-4E protein does not accumulate elsewhere in the muscles of *pum* mutants (Figures 4H and 4I). This is consistent with the fact that Pum protein in muscles is restricted to the NMJ region (Figure 2).

eIF-4E overexpression in muscles produces an increase in the number of boutons, perhaps due to the recruitment of new active zones to sites of local translation (Sigrist et al., 2000). If Pum represses eIF-4E synthesis at the NMJ, one might expect that simultaneous elevation of muscle Pum levels would suppress the increase in Ib bouton number produced by crossing UAS-eIF-4E to a muscle-specific driver. This is in fact the case (Figure 5C).

New and brighter GluRIIA puncta appear in response to increases in larval motor activity or to genetic manipulations of *eIF-4E* or *pabp*. These changes in receptor expression do not lead to an increase in postsynaptic responsiveness to transmitter, as measured by mEJP amplitude. They do, however, increase evoked transmitter release. The frequency of spontaneous transmitter release (mEJP frequency) also increases, and additional active zones accumulate at each NMJ. These results suggest that the additional GluRIIa puncta recruit new active zones through a retrograde signaling mechanism and that the new active zones have a normal density of functional receptors. The same effects are observed when GluRIIa is overexpressed in muscles (Sigrist et al., 2000, 2002, 2003).

To examine the downstream effects caused by removal of Pum and the consequent increase in eIF-4E aggregates, we stained *pum* mutant larvae for GluRIIa. We observed a dramatic increase in the number and intensity of receptor puncta (Figure 7). This result suggests that synaptic *GluRIIa* mRNA may be translated more efficiently or is more stable at NMJs lacking *pum* function.

When examined by electrophysiology, *pum* mutant NMJs display elevated mEJP frequencies, suggesting that the extra GluRIIa puncta seen in these larvae may also define additional active zones. The increase in mEJP frequency (2- to 3-fold) seen in *pum* mutants (Figure 8C) is greater than that observed in the genotypes studied by Schuster and colleagues (1.5-fold) (Sigrist et al., 2002). However, in contrast to their results with GluRIIa overexpression, we saw no corresponding increase in the evoked response in a *pum* mutant in which Pum had been restored to neurons (Figure 8A).

We did see an increase in the number of Is boutons in *pum* mutants, and this phenotype was rescued by postsynaptic Pum expression (Figure 5D). Since Is boutons were particularly rich in GluRIIa puncta in *pum* mutants (Figure 7), one might have expected that new active zones that mediate evoked responses would exist at these supernumerary boutons. However, perhaps postsynaptic defects caused by dysregulation of other, as yet undefined, Pum mRNA targets impair the ability of the new GluRII puncta to increase the evoked response.

Neuronal Pumilio Regulates Synaptic Growth and Morphology

The morphologies of the Ib and Is NMJs are both regulated by Pum, but in opposite directions and from opposite sides of the synapse. Ib boutons are decreased in number in *pum* LOF mutants, and this phenotype is rescued by restoring Pum in neurons (Figure 3); Is boutons are increased in number, and this phenotype is rescued by postsynaptic Pum (Figure 5D).

The divergent Ib NMJ phenotypes produced by loss and overexpression of Pum in neurons suggest that Pum has an instructional role in controlling the growth and morphology of these presynaptic terminals (Figure 3). Loss of *pum* function and overexpression of Pum also have divergent effects on the morphologies of dendrites. In larval peripheral sensory neurons, Pum overexpression produces a reduction in higher-order dendritic branches, while loss of *pum* function causes an increase in the length of dendritic spikes (Ye et al., 2004). The morphological changes observed in presynaptic terminals and dendrites when *pum* function is reduced or elevated suggest that it might directly or indirectly repress translation of mRNAs encoding cytoskeletal components.

A gene encoding a cytoskeletal protein has been characterized whose mutant phenotypes parallel those of *pum*. *DVAP-33A* LOF mutations and DVAP-33A neuronal overexpression produce phenotypes like the *pum* LOF and neuronal overexpression phenotypes we describe here. *DVAP-33A* mutations affect the structure of the synaptic microtubule cytoskeleton (Pennetta et al., 2002), and microtubules are altered in a similar manner in the NMJs of *pum* LOF mutants (data not shown). These findings do not suggest that *DVAP-33A* is a target of Pum repression but may indicate that it is required for Pum-regulated presynaptic functions.

Electrophysiological studies have suggested that ion channels might be targets of Pum regulation. The hypomorphic pum^{bem} mutation does not produce changes in basal synaptic transmission at the NMJ, but persistent facilitation in motor neurons is prematurely induced by repetitive nerve stimulation (Schweers et al., 2002). Facilitation is also produced by neuronal overexpression of the *para* Na^+ channel or by LOF mutations in the *Hyperkinetic* K^+ channel gene, so dysregulation of these or other channels could explain the pum^{bem} phenotype (Stern and Ganetzky, 1989; Stern et al., 1990).

It is likely that phenotypes caused by loss of neuronal Pum are complex, arising from the combined derepression of several different targets. Expression of Pum itself might be regulated by environmental conditions, since it has been found that *pum* mRNA levels increase in the adult *Drosophila* brain under conditions favoring long-term memory formation (Dubnau et al., 2003).

In summary, Pum-mediated posttranscriptional regulation is likely to be important for synaptic morphology and function in both larvae and adults. Pum has distinct roles on the presynaptic and postsynaptic sides of the larval NMJ. Synaptic regulatory pathways involving Pum might be conserved in mammals, since mammalian Pum proteins are very similar in sequence to fly Pum and are expressed in the brain.

Experimental Procedures

Genetics

Wild-type controls were either w^{1118} or *Elav-Gal4* crossed to w^{1118} or *MHC-GAL4* crossed to *w1118*, depending on the experiment. *UAS-Pum RBD*, *UAS-Pum* (full-length), and *UAS-Pum* (full-length)-*tub 3′UTR* flies were generated by standard techniques. *MHC-Gene-Switch-GAL4* (*MHC-GSGAL4*) was obtained from Thomas Osterwalder and Haig Keshishian (Osterwalder et al., 2001). *Elav-Gal4 (II)* and *MHC-CD8-Shaker-GFP* flies were obtained from Corey Goodman's group (Zito et al., 1999). For neuronal and muscle rescue crosses, *UAS-pum* and *UAS-pum-tubulin 3′UTR* insertions were recombined with pum^{ET7}, and *MHC-GSGAL4* was recombined with pum^{ET9}. *Df(3R)BSC24* (Bloomington Stock Center) has breakpoints at 85C4-9 and 85D12-14.

All crosses to generate wild-type and *pum* larvae including rescue crosses and appropriate controls were done at 18°C, since *pum* defects are strongest at that temperature; overexpression crosses and appropriate controls were done at 29°C. *UAS-eIF-4E* flies were obtained from Christoph Schuster (Sigrist et al., 2000). Crosses to test genetic interactions between *eIF-4E* and *pum* were done at 25°C. Details concerning lethality produced by Pum overexpression are in the Supplemental Data at http://www.neuron.org/cgi/content/full/44/4/663/DC1/.

Antibodies

The following primary antibodies were used in this study: rabbit anti-PumN (Forbes and Lehmann, 1998), rat anti-Pum RBD (Sonoda and Wharton, 1999), monoclonal anti-Synaptotagmin mAb 3H2 (Menon and Zinn, 1998), rabbit anti-Dlg (from Peter Bryant), mouse anti-Dlg mAb (from Corey Goodman), monoclonal anti-Elav and anti-Fasciclin II mAb 1D4 (Developmental Studies Hybridoma Bank), monoclonal anti-Futsch mAb 22C10 (from S. Benzer), rabbit anti-eIF-4E (from P. Lasko; see Sigrist et al., 2000), rabbit anti-GluRIIa DM2 (from Y. Kidokoro; Saitoe et al., 1997), and rabbit anti-GluRIIB and anti-GluRIII (Marrus et al., 2004). Secondary antibodies were from Molecular Probes, OR: Alexa Fluor 568 anti-rabbit, Alexa Fluor 568 anti-rat, and Alexa Fluor 488 anti-mouse antibodies were preabsorbed against wild-type embryos and then used at a concentration of 1:500.

Immunocytochemistry

Third instar larvae were dissected in standard HL-3 Ringer's solution and fixed in 4% paraformaldehyde or Bouin's fix (Sigma). Laser scanning confocal microscopy was performed on a Zeiss 510 microscope. Maximum intensity projections were generated from stacks collected with intervals of 0.7 μm in all cases except for Figure 5, where the interval was 0.4 μm. Figures 4G and 2E are single confocal sections; images in all other figures are projections of confocal z series stacks. Images were combined using Adobe Photoshop.

Detailed methods for (1) quantitating Pum levels at the NMJ; (2) quantitative evaluation of synaptic phenotypes; (3) induction of larval movement and quantitation of eIF-4E; and (4) staining for GluRIIa are in the Supplemental Data at http://www.neuron.org/cgi/content/full/44/4/663/DC1/.

RNA Binding Assays

Binding experiments were performed essentially as described by Wharton et al. (1998) with 30 fmol or less of end-labeled RNA per 10 μl reaction. The mutant *hb* binding site (UG21AC of Wharton et al., 1998) bears two substitutions in the critical UGU trinucleotide. The *eIF-4E* sequences were prepared by separate PCR amplification of nt 1–130 and 131–252 of clone SD5406, which contains four nucleotides that do not match the genomic *eIF-4E* sequence and probably are polymorphisms.

Electrophysiology

For all genotypes (wild-type, *pum* LOF, *pum* rescues, and corresponding controls) third instar larvae were taken from culture medium, from crosses that were set up at 18°C. Electrophysiological recordings were performed as described previously (Stimson et al., 1998). Briefly, larvae were dissected in HL3 ringers (with 1 mM Ca^{2+}). Recording electrodes were heat-pulled fiber-filled glass capillaries with tip resistances between 20 and 25 MΩ. EJPs were recorded in the bridge mode using an axoclamp-2B amplifier. EJPs were recorded from muscle 6 in abdominal segment 2 following a suprathreshold stimulation to the innervating motor axons at 1 Hz. Only recordings where the muscle resting membrane potential was at least −60 mV were considered. Mean EJP amplitude was determined by averaging 20 sequential EJPs. EJP amplitudes were corrected for nonlinear summation using the formula in Feeney et al. (1998). Spontaneous events were also monitored for a period of 50 s. The mean mEJP amplitude and frequency were calculated from these traces using the mini-analysis software (Synaptosoft, Inc). Statistical analysis including graphing and test of significance (paired Student's t tests) were performed in Sigma Plot (Jandel Scientific). Quantal content was calculated by dividing the mean corrected EJP amplitude by the mean mEJC amplitude in each case.

Acknowledgments

We thank the members of the Zinn group and Erin Schuman, Christoph Schuster, Aaron DiAntonio, Chand Desai, and Ruth Lehmann for helpful discussions. We thank Thomas Osterwalder and Haig Keshishian for GeneSwitch flies; Christoph Schuster and Paul Lasko for eIF-4E antibody and transgenic lines; Ruth Lehmann for anti-PumN; Yoshiaki Kidokoro for GluRIIa antibody; Aaron DiAntonio for GluRIIB and GluRIII antibodies; Dan Woods and Peter Bryant for Discs-large antibody; Murim Choi for making the Pum transgenic lines; Anna Salazar, Elena Armand, and Chin-Yin Tai for assistance with Western blotting; and W. Bryan Smith for help with Image J software. Confocal imaging was performed at the Caltech Biological Imaging Facility. This work was supported in part by NIH RO1 grant NS43416 to K.Z.; and by grants DA15495 and DA15383 to M.R. S.S. was supported in part by grant NIH T32 CA09213.

Received: November 5, 2003
Revised: June 26, 2004
Accepted: October 6, 2004
Published: November 17, 2004

References

Chagnovich, D., and Lehmann, R. (2001). Poly(A)-independent regulation of maternal hunchback translation in the *Drosophila* embryo. Proc. Natl. Acad. Sci. USA *98*, 11359–11364.

Dubnau, J., Chiang, A.S., Grady, L., Barditch, J., Gossweiler, S., McNeil, J., Smith, P., Buldoc, F., Scott, R., Certa, U., et al. (2003). The staufen/pumilio pathway is involved in *Drosophila* long-term memory. Curr. Biol. *13*, 286–296.

Feeney, C.J., Karunanithi, S., Pearce, J., Govind, C.K., and Atwood, H.L. (1998). Motor nerve terminals on abdominal muscles in larval flesh flies, Sarcophaga bullata: comparisons with Drosophila. J. Comp. Neurol. *402*, 197–209.

Forbes, A., and Lehmann, R. (1998). Nanos and Pumilio have critical roles in the development and function of Drosophila germline stem cells. Development *125*, 679–690.

Jiang, C., and Schuman, E.M. (2002). Regulation and function of local protein synthesis in neuronal dendrites. Trends Biochem. Sci. *27*, 506–513.

Keshishian, H., Broadie, K., Chiba, A., and Bate, M. (1996). The *Drosophila* neuromuscular junction: A model for studying development and function. Annu. Rev. Neurosci. *19*, 545–575.

Koh, Y.H., Gramates, L.S., and Budnik, V. (2000). Drosophila larval neuromuscular junction: molecular components and mechanisms underlying synaptic plasticity. Microsc. Res. Tech. *49*, 14–25.

Kraut, R., Menon, K., and Zinn, K. (2001). A gain-of-function screen for genes controlling motor axon guidance and synaptogenesis in *Drosophila*. Curr. Biol. *11*, 417–430.

Lnenicka, G.A., and Keshishian, H. (2000). Identified motor terminals in Drosophila larvae show distinct differences in morphology and physiology. J. Neurobiol. *43*, 186–197.

Marrus, S.B., Portman, S.L., Allen, M.J., Moffat, K.G., and DiAntonio, A. (2004). Differential localization of glutamate receptor subunits at the Drosophila neuromuscular junction. J. Neurosci. *24*, 1406–1415.

Menon, K.P., and Zinn, K. (1998). Tyrosine kinase inhibition produces specific alterations in axon guidance in the grasshopper embryo. Development *125*, 4121–4131.

Murata, Y., and Wharton, R.P. (1995). Binding of Pumilio to maternal hunchback mRNA is required for posterior patterning in *Drosophila* embryos. Cell *80*, 747–756.

Nakahata, S., Katsu, Y., Mita, K., Inoue, K., Nagahama, Y., and Yamashita, M. (2001). Biochemical identification of Xenopus Pumilio as a sequence-specific cyclin B1 mRNA-binding protein that physically interacts with a Nanos homolog, Xcat-2, and a cytoplasmic polyadenylation element-binding protein. J. Biol. Chem. *276*, 20945–20953.

Osterwalder, T., Yoon, K.S., White, B.H., and Keshishian, H. (2001). A conditional tissue-specific transgene expression system using inducible GAL4. Proc. Natl. Acad. Sci. USA *98*, 12596–12601.

Parisi, M., and Lin, H. (1999). The Drosophila pumilio gene encodes two functional protein isoforms that play multiple roles in germline development, gonadogenesis, oogenesis and embryogenesis. Genetics *153*, 235–250.

Pennetta, G., Hiesinger, P.R., Fabian-Fine, R., Meinertzhagen, I.A., and Bellen, H.J. (2002). *Drosophila* VAP-33A directs bouton formation at neuromuscular junctions in a dosage-dependent manner. Neuron *35*, 291–306.

Petersen, S.A., Fetter, R.D., Noordermeer, J.N., Goodman, C.S., and DiAntonio, A. (1997). Genetic analysis of glutamate receptors in *Drosophila* reveals a retrograde signal regulating presynaptic transmitter release. Neuron *19*, 1237–1248.

Roman, G., Endo, K., Zong, L., and Davis, R.L. (2001). P{Switch}, a system for spatial and temporal control of gene expression in Drosophila melanogaster. Proc. Natl. Acad. Sci. USA *98*, 12602–12607.

Rorth, P., Szabo, K., Bailey, A., Laverty, T., Rehm, J., Rubin, G.M., Weigmann, K., Milan, M., Benes, V., Ansorge, W., and Cohen, S.M. (1998). Systematic gain-of-function genetics in Drosophila. Development *125*, 1049–1057.

Saitoe, M., Tanaka, S., Takata, K., and Kidokoro, Y. (1997). Neural activity affects distribution of glutamate receptors during neuromuscular junction formation in *Drosophila* embryos. Dev. Biol. *184*, 48–60.

Schweers, B.A., Walters, K.J., and Stern, M. (2002). The *Drosophila melanogaster* translational repressor Pumilio regulates neuronal excitability. Genetics *161*, 1177–1185.

Sigrist, S.J., Thiel, P.R., Reiff, D.F., Lachance, P.E.D., Lasko, P., and Schuster, C.M. (2000). Postsynaptic translation affects the efficacy and morphology of neuromuscular junctions. Nature *405*, 1062–1065.

Sigrist, S.J., Thiel, P.R., Reiff, D.F., and Schuster, C.M. (2002). The postsynaptic glutamate receptor subunit DGluR-IIA mediates long-term plasticity in Drosophila. J. Neurosci. *22*, 7362–7372.

Sigrist, S.J., Reiff, D.F., Thiel, P.R., Steinert, J.R., and Schuster, C.M. (2003). Experience-dependent strengthening of Drosophila neuromuscular junctions. J. Neurosci. *23*, 6546–6556.

Sonenberg, N., and Gingras, A.-C. (1998). The mRNA 5′ cap-binding protein eIF4E and control of cell growth. Curr. Opin. Cell Biol. *10*, 268–275.

Sonoda, J., and Wharton, R.P. (1999). Recruitment of Nanos to hunchback mRNA by Pumilio. Genes Dev. *13*, 2704–2712.

Sonoda, J., and Wharton, R.P. (2001). Drosophila Brain Tumor is a translational repressor. Genes Dev. *15*, 762–773.

Spassov, D.S., and Jurecic, R. (2003). Mouse Pum1 and Pum2 genes, members of the Pumilio family of RNA-binding proteins, show differential expression in fetal and adult hematopoietic stem cells and progenitors. Blood Cells Mol. Dis. *30*, 55–69.

Stern, M., and Ganetzky, B. (1989). Altered synaptic transmission in *Drosophila hyperkinetic* mutants. J. Neurogenet. *5*, 215–228.

Stern, M., Kreber, R., and Ganetzky, B. (1990). Dosage effects of a Drosophila sodium channel gene on behavior and axonal excitability. Genetics *124*, 133–143.

Steward, O., and Schuman, E.M. (2001). Protein synthesis at synaptic sites on dendrites. Annu. Rev. Neurosci. *24*, 299–325.

Stimson, D.T., Estes, P.S., Smith, M., Kelly, L.E., and Ramaswami, M. (1998). A product of the Drosophila stoned locus regulates neurotransmitter release. J. Neurosci. *18*, 9638–9649.

Wells, D.G., Dong, X., Quinlan, E.M., Huang, Y.-S., Bear, M.F., Richter, J.D., and Fallon, J.R. (2001). A role for the cytoplasmic polyadenylation element in NMDA receptor-regulated mRNA translation in neurons. J. Neurosci. *21*, 9541–9548.

Wharton, R.P., Sonoda, J., Lee, T., Patterson, M., and Murata, Y. (1998). The Pumilio RNA-binding domain is also a translational regulator. Mol. Cell *1*, 863–872.

Wickens, M., Bernstein, D.S., Kimble, J., and Parker, R. (2002). A PUF family portrait: 3′UTR regulation as a way of life. Trends Genet. *18*, 150–157.

Ye, B., Petritsch, C., Clark, I.E., Gavis, E.R., Jan, L.Y., and Jan, Y.N. (2004). Nanos and Pumilio are essential for dendrite morphogenesis in *Drosophila* peripheral neurons. Curr. Biol. *14*, 314–321.

Zamore, P.D., Bartel, D.P., Lehmann, R., and Williamson, J.R. (1999). The PUMILIO-RNA interaction: A single RNA-binding domain monomer recognizes a bipartite target sequence. Biochemistry *38*, 596–604.

Zito, K., Parnas, D., Fetter, R.D., Isacoff, E.Y., and Goodman, C.S. (1999). Watching a synapse grow: Noninvasive confocal imaging of synaptic growth in *Drosophila*. Neuron *22*, 719–729.